Heat of Adsorption of Butane on Multiwalled Carbon Nanotubes

Jenny M. Hilding and Eric A. Grulke*

Department of Chemical and Materials Engineering, University of Kentucky, 177 Anderson Hall, Lexington, Kentucky 40506-0046

Received: August 11, 2003; In Final Form: April 27, 2004

We report the isosteric heats of adsorption, q_{st}, for butane on multiwalled carbon nanotubes (MWNTs) over a range of surface loadings at temperatures below the normal boiling point. Butane is a nonspherical, nonpolar molecule that may exhibit different orientations in multilayer adsorption. The morphology of our MWNTs is such that only surface adsorption or capillary condensation can occur: no interstitial sites between nanotubes are available to butane. For these nanotubes, exterior surface adsorption is the principal mechanism measured by gravimetric analysis as the internal pores are only a small volume fraction of the total solid volume. The isosteric heat of adsorption varied with the surface coverage, θ, defined as the ratio of adsorbed butane to the MWNT butane monolayer capacity. The initial heat of adsorption was in the region ~22−26 kJ/mol, which is approximately $^1/_3$ lower than the corresponding value for various graphite−butane systems. At $\theta = 1$, q_{st} displays a minima (13.5−15.9 kJ/mol). The isosteric heat of adsorption approaches the butane heat of condensation for $\theta > 2.5$, suggesting that the surface film is similar to a bulk phase. The isosteric heat of adsorption of butane on MWNTs can be related to the morphology of the MWNTs. The higher heats of adsorption at low coverages are likely related to the presence of surface defects. The minima in q_{st} near the monolayer coverage relates to a high self-association of butane. At high loadings, the butane surface film is similar to a bulk phase.

Introduction

Carbon nanotubes (CNTs) are relatively inert materials, possessing unique structural and mechanical properties.[1] They have been proposed as adsorbents for a variety of gases, from hydrogen to alkanes to fluorocarbons. Nanotubes have a well-defined, simple geometry, with the tube wall consisting of curved graphite sheets forming tubes with a diameter and length on the nano- and microscale, respectively. Single-walled nanotubes (SWNT) consist of only one carbon layer, while multiwalled carbon nanotubes (MWNT) consist of at least two layers.

The SWNTs have pores in the microporous range and often self-assemble in small bundles with hexagonal packing, thus generating organized SWNT "macrostructures". These structures contain a number of different adsorption sites with different adsorption potentials. Adsorption can occur on the SWNT external wall surface as well as in the external bundle grooves created between neighboring SWNTs. Smaller adsorbates tend to adsorb in the interstitial channels[2−4] generated between the SWNTs, a capillary condensation phenomenon rather than a surface adsorption effect. In the same manner, the adsorbate may also condense in the SWNT pores.

MWNTs generally have pores in the mesoporous range (between 20 and 500 Å) and typically do not form ordered solids with interstitial sites. This means that usually there are only two types of adsorption sites available in a MWNT system, assuming that at least one end is accessible to the atmosphere, which results in either external surface adsorption or capillary condensation in the MWNT channel.

Internal pore volumes and external surface areas can be quantitatively determined from measurements of SEM- or TEM-microphotographs. Therefore, adsorption and desorption of gases on these solids should be easily analyzed and computed from heats of adsorption and morphology information, facilitating the design of adsorption systems. As we have previously demonstrated, both the MWNT length and inner and outer diameter distributions can be successfully fitted with a log-normal distribution model.[1,5] MWNTs have an estimated layer-to-layer spacing of 0.34 nm,[6] which means that whereas a molecule like butane is small enough to condense in the MWNT pore, it is too large to adsorb between the MWNT layers.

Experimental Section

The MWNT samples used in the experiments were produced at the Center for Applied Energy Research (CAER), Lexington, KY. These MWNTs are produced through a chemical vapor deposition process (CVD[7,8]), which gives samples with uniform lengths and high purity (>95 wt %). The impurities mainly consist of residual catalyst (ferrocene) and some smaller amounts of amorphous carbon and soot. As the MWNTs are cut from their growth positions on the substrate surface, all nanotubes are assumed to have at least one end open to the atmosphere. The CAER samples generally have inner diameters ranging from 2 to 12 nm and external diameters between 12 nm and up to ~400 nm.[5] The lengths are usually very similar between the MWNTs within a sample. Three different samples with average lengths of 50−55 μm were used. It was assumed that the three samples had slightly different morphologies, a consequence of altering the process parameters between production runs. These three samples were compared to three similar samples with previously analyzed and well-defined morphology.[5] The purpose of this procedure was to assess the possibility of adsorption as a tool to determine a MWNT sample's morphology, instead of using time-consuming and complicated TEM analysis.

* To whom correspondence should be addressed. E-mail: egrulke@engr.uky.edu.

10.1021/jp036387k CCC: $27.50
Published on Web 08/18/2004

The adsorption experiments were carried out with an Intelligent Gravimetrical Analysis instrument (IGA-002, Hiden Analytical Ltd.) designed specifically for organic vapor adsorption studies. A sample of approximately 50 mg was hung in a small quartz bulb connected to a microbalance. Water and other unwanted adsorbed gases were removed by heating the system to 473.15 K at atmospheric pressure. At this temperature, the vapor pressure of water in the MWNT pores exceeded the saturation conditions, as calculated from the Kelvin equation[9,10] and the DIPPR[11]-data set.

After degassing, the system was cooled to an initial temperature of 278.15 K for adsorption studies. The pressure of the system was decreased to a relative butane pressure on the order of 1×10^{-3}. The system was left until the sample weight was stabilized. High-purity butane was allowed to flow over the sample and the new weight was noted after stabilization. The pressure was increased in small increments of 0.05% of the pressure span and the sample was allowed to reach equilibrium after each step. The minimum hold time was set at 5 min. Typical pressure changes take about 15 s to be achieved. Generally, it would take less than 30 s to reach 95% of the maximum uptake for one pressure step, which is nearly the amount of time needed for the instrument to set the new pressure. When the mass or pressure fluctuations are less than 0.02% of the span, the sample is deemed to be at equilibrium and the next step is taken. This procedure continued until the system reached the maximum cycle pressure of ~90% of the saturated vapor pressure, $p°$, for butane at current temperature. Desorption curves were obtained permitting pressure reductions to low final pressures.

The microbalance/microbalance controller of the IGA-002 has an intrinsic accuracy equivalent to ±0.006% of the selected weighing range (100 mg in this case). The pressure control system can typically maintain a pressure set-point to within 0.02% of the operating range. The thermo-regulator has an accuracy of at least ±0.1 °C and the intrinsic resolution of the temperature sensor is in the range of 0.1−0.25 K.

After each completed pressure cycle, the system temperature was increased 5 or 10 deg K and the system was allowed to reach equilibrium before measuring a new isotherm. This procedure was repeated 3−4 times for each sample, each procedure generating a different isotherm. The temperatures were kept in a range of 278.15−308.15 K.

Data Analysis and Discussion

We have previously shown that our butane−MWNT adsorption systems generate isotherms of type II,[5] which is defined as physisorption of a gas on a nonporous solid. Theoretically, the adsorption capacity should be higher for a solid with a larger surface area (m^2/g). For our MWNT samples, surface area per weight directly corresponds to the sample's average external diameter (D_O); smaller average diameters correlate to larger surface areas.[5] The generated isotherms are of type II, and show that sample 1 has the largest adsorption capacity, closely followed by samples 2 and 3 (Figure 1), so we conclude that $D_{O1} < D_{O2} < D_{O3}$. This result indicates that sample 1 has the smallest average diameter, followed by sample 2, and then sample 3. The possibility of establishing a MWNT sample's morphology from isotherm data will be investigated and discussed in depth further.

Each sample's isotherms can be thoroughly analyzed with the aid of three well-known equations. The modified BET[12] equation models type II isotherms, the Kelvin equation predicts the occurrence of capillary condensation in a porous system,

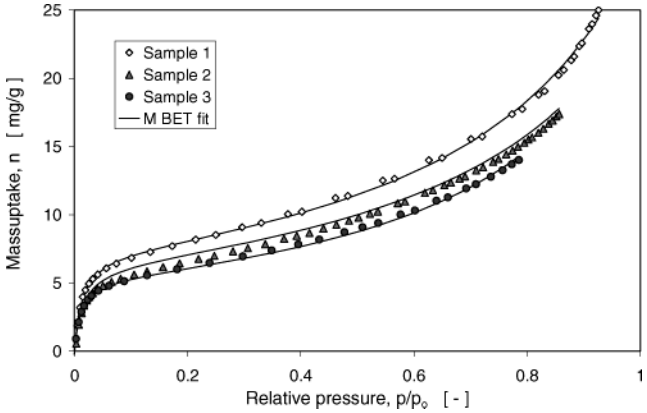

Figure 1. Adsorption isotherms at $T = 298.15$ K plotted together with modified BET model fits for three different samples.

TABLE 1: The Modified BET Equation Fitting Parameters for Isotherms Measured from Samples 1−3 for Several Temperatures

		temp [K]					
sample	coefficient	278	283	288	293	298	308
1	n_m [mg/g]	6.71		6.64		7.20	7.32
	K	0.78		0.78		0.76	0.72
	C	104		109		100	89
2	n_m [mg/g]	6.0		6.1		6.3	6.6
	K	0.78		0.80		0.75	0.76
	C	117		128		92	94
3	n_m [mg/g]	5.18	5.05	5.10	5.35	5.29	
	K	0.82	0.82	0.82	0.81	0.80	
	C	134	100	105	128	116	

and the Clausius−Clapeyron equation is used to calculate the heat of adsorption from a set of isotherms. Here follows a brief presentation of each equation together with the analysis and discussion of our data.

Adsorption Model. The modified BET equation is generally applicable to adsorbents with pores in the mesoporous range and it predicts adsorbed mass, n, as a function of relative pressure, $p/p°$, where p is the system pressure and $p°$ is the adsorbate vapor pressure at system temperature:

$$n = n_m \frac{ck\frac{p}{p^o}}{\left(1 - k\frac{p}{p^o}\right)\left(1 + k(c-1)\frac{p}{p^o}\right)} \text{ g/g} \qquad (1)$$

Equation 1 is based on the parameters n_m, c, and k, where n_m represents the monolayer capacity, and c and k correspond to the adsorption capacity. The DIPPR data set[11] was used to determine all the butane physical properties at different temperatures.

Model coefficients were fitted with use of Maple mathematical software program. The modified BET fits were excellent, as shown in Figure 1. The BET modeling parameters for each isotherm fit are presented in Table 1. The monolayer capacity, n_m, increased slightly with system temperature, while k decreased with T. The parameter c seems to change inconsistently with T. The modified BET equation has previously been used to fit the isotherms for a large number of different CH/carbon black systems. The parameter c was found to be approximately 100 for all of the systems,[13] which means that our c values are consistent with other research groups' findings. For our system, the modified BET model is relatively insensitive to parameter c.

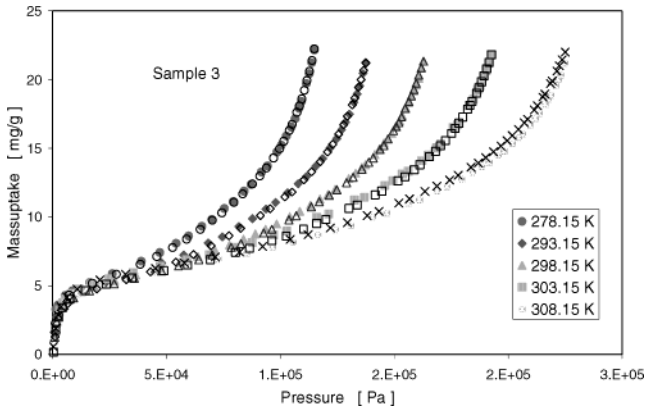

Figure 2. Five different, complete sample 3 adsorption−desorption cycles. The adsorption and desorption isotherms are represented by filled and empty symbols, respectively.

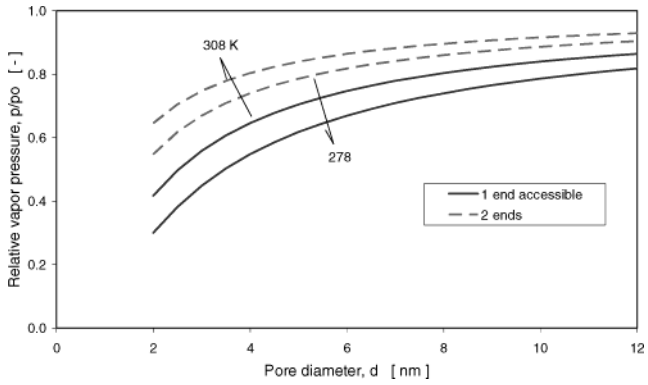

Figure 3. Capillary condensation in MWNTs as a function of MWNT pore diameter and temperature according to the Kelvin equation (eq 2). The monolayer coverage, n_m, is complete at a relative pressure of approximately 0.05, so the capillary condensation occurs first after the initial monolayer is complete.

Condensation in MWNT Pores. If the gas phase relative pressure is increased over the range 0−1, capillary condensation will occur in the smaller pores initially and continue to the larger pores as the pressure increase continues. The Kelvin equation predicts that the vapor pressure over a concave meniscus is lower than the saturation vapor pressure, p°, over a flat surface.[9,10] For cylindrical pores, the Kelvin equation is written:

$$\left(\frac{p}{p^{\circ}}\right)_{\text{ads}} = \mathrm{e}^{(-2\gamma V_{\mathrm{L}}/RTr_m)} \qquad (2)$$

V_L is the liquid molar volume, p/p° is the adsorbate relative pressure, and γ is the surface tension. Equation 2 is thought to give good predictions of vapor pressures in pores down to 2 nm in diameter. As mentioned earlier, the MWNTs used here are mesoporous with respect to their capillary diameter and the harvest method ensures that at least one tube end is open. Butane is small enough to adsorb through capillary condensation in a mesoporous material, and for our MWNTs, the sample porosity is confirmed to be a function strictly of accessible nanotube pores. Our adsorption/desorption isotherms show no detectible hysteresis, as seen in Figure 2, where five different isotherm cycles, generated for sample 3, are presented.

The capillary condensation process is highly dependent on pore accessibility. When a cylinder is open at both ends, the meniscus is cylindrical and formed over the cylinder surface ($2\pi rL$), so that the radius of the meniscus, r_m, equals $2r$, where r is the pore radius. The capillary condensation has to be nucleated by the monolayer film on the pore wall. This process is spontaneous, since the pore radius decreases as the condensation progresses, which in turn further decreases the vapor pressure. If the cylinder is accessible at one end only, the meniscus is hemispherical over the closed end, rather than cylindrical over the tube walls, and r_m is now equal to r.

The course of events is slightly different for the desorption process. The evaporation takes place from a hemispherical meniscus for both types of tube. As a consequence, condensation and evaporation take place at different relative pressures for a tube open at both ends. A hysteresis loop in the adsorption/desorption cycle could be the result of two accessible ends. The lack of hysteresis in our systems could indicate that the majority of the MWNTs present have only one accessible tube end. Other groups have reported a lack of hysteresis for the nitrogen/MWNT[14] and methane/MWNT[15] systems. Activated MWNTs do show hysteresis on adsorption of methane and nitrogen. The activation process most likely opens up the nanotube ends (the end being the most reactive site due to the high local curvature) hence creating cylindrical menisci. Activated carbons generally show condensed material, which cannot be recovered during desorption.

Another explanation could be that the pore capacity is too small to be seen as a hysteresis loop, since, according to the Kelvin equation, capillary condensation takes place in the relative pressure range of 0.3−0.93 (T = 273−308 K) in pores with diameters between 2 and 12 nm (Figure 3). Calculations show that only about 0.5 wt % of the total mass uptake is condensed in the actual pore of the smallest diameter MWNT, and this amount decreases with increasing wall thickness/tube size.[5] Compared to MWNTs, SWNTs have higher pore volume densities. Hysteresis is generally present in SWNT-adsorbent systems, but is not common for MWNT systems. The SWNT diameter range is basically a Poisson distribution in the micropore range, which means that the capillary condensation occurs in a narrow relative pressure region for SWNTs ($p/p^\circ \approx$ 0.1−0.3) compared to MWNTs. It is also of interest to recall that the interstitial channels generally present in SWNT systems are open at both ends, which leads us back to the discussion regarding pore accessibility.

Isosteric Heat of Adsorption. The pressure at which a sample adsorbs a specific mass when the temperature is kept constant can be easily calculated from the modified BET fit for the isotherm corresponding to T. These data can in turn be used to calculate q_{st} from the Clasius−Clapeyron equation (eq 3), which predicts the isosteric heat of adsorption, q_{st}, as a function of pressure and temperature for a fixed mass uptake. The equation is based on the assumption that the adsorbate is an ideal gas and adsorbs with negligible volume.

$$q_{\mathrm{st}} = -\Delta h_{\mathrm{a}} = RT^2\left(\frac{\partial \ln p}{\partial T}\right)_{\mathrm{na}} \text{ J/mol} \qquad (3)$$

Data sets from at least two different isotherms per sample are necessary for eq 3 to be applicable. T and p are system temperature and pressure at a fixed mass uptake, n_a, and R is the universal gas constant. Figure 4 shows a set of different adsorption isotherms plotted together with corresponding modified BET fit.

The calculated isosteric heats of adsorption of the three samples are presented in Figure 5, where q_{st} is plotted vs relative monolayer coverage ($\theta = n_a/n_m$). The isosteric heat of adsorption is high at very low coverage, decreases steadily, and has a minimum just as the monolayer reaches its completion and θ equals 1. Finally, q_{st} approaches the heat of condensation for butane[11] at $\theta \approx 2.5$. The shaded field in Figure 5 represents the

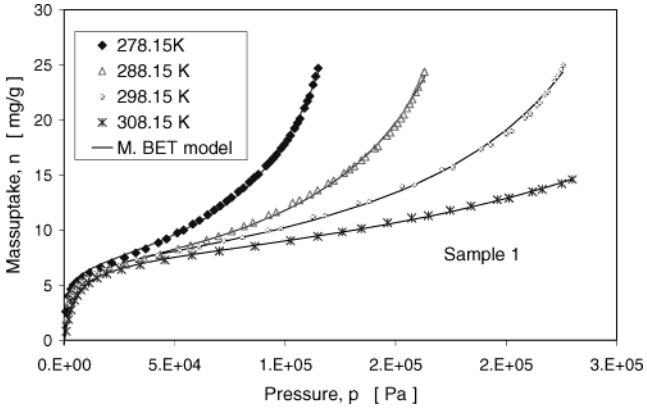

Figure 4. A set of adsorption isotherms for a sample (sample 1) recorded at constant temperatures between 278 and 308 K. If the adsorption data is plotted vs relative pressure ($p/p°$), the isotherms collapse to one curve.

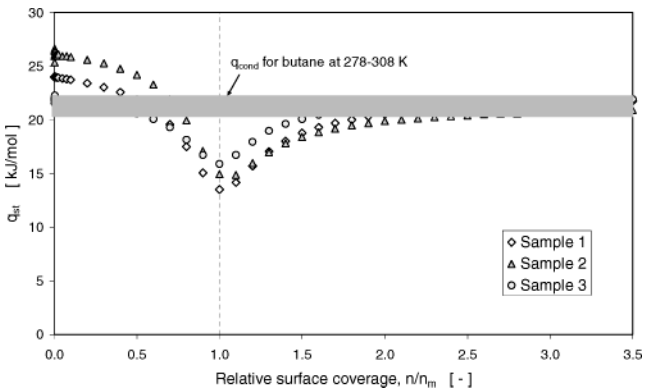

Figure 5. The isosteric heats of adsorption for samples 1−3 are plotted vs relative mass uptake, θ or n/n_m.

butane heat of condensation between 278 and 308 K, the temperature range for our data.

For a homogeneous surface, q_{st} generally increases steadily with θ, from $\theta \approx 0$ up to a maximum right before the monolayer completion. This increase in q_{st} is a consequence of adsorbate−adsorbate interactions. In reality, there are no perfectly homogeneous adsorbents, but graphitized carbon black consists mainly of (001) planes and a low percentage of sites with higher energy.

Heterogeneous sites give q_{st} curves that are high at low fractional coverage and then quickly drop as the more highly energetic active sites are occupied. This behavior has been observed for ethylene,[16] methane, Xe, and N_2 adsorption on graphite.[17] For these systems, the q_{st} curve displays a sharp submonolayer minimum, likely caused by the energetic heterogeneity of the adsorbate surface. After the drop, q_{st} increases as a result of the interactions between the adsorbate molecules. When the first layer is complete, q_{st} drops dramatically again.

The fact that the isosteric heat of adsorption is highest initially and starts to decrease immediately suggests that the MWNT samples are heterogeneous adsorbents. Since the sample labeling is in order of the sample's mean external diameters, we can see that q_{st} does not correlate to the nanotube morphology at low surface coverage. It is likely that the initial heat of adsorption depends more on surface structure than on the nanotube diameter; the defects on the MWNTs most likely dominate the initial stages of the adsorption. Several studies suggest that defect sites are of great importance to the adsorption process. The impact can be seen not only in systems where nanotubes[18−22] or other carbon materials[23,24] are used as the adsorbate, but also for metallic crystalline materials.[25,26] It is not likely that the defects are reactive to butane, as chemisorption generally causes hysteresis or even irreversible adsorption.

At low surface coverage, q_{st} is higher than the heat of condensation. Lennard-Jones 6−12 potential calculations show that the attractive force between butane molecules is much stronger than it is between butane and carbon. Also, butane incompletely wets graphite.[27] These data suggest that the structure in the monolayer region is different from the structure in the multilayer region. At $\theta \approx 2.5$, the isosteric heats of adsorption are essentially the same for all our samples, with values in the immediate vicinity of butane's heat of condensation. Since the butane molecules in the upper layers are surrounded by other butane molecules only, the result is not unexpected. This finding also indicates that approximately two monomolecular butane layers are sufficient to screen butane molecules from the effects of the MWNT surface. The result is consistent with previous work with butane adsorption near its melting point; multilayer films formed at $\theta \approx 2.65$ on graphite foam[28] and at $\theta \approx 2.0$ on Paypex.[27] The first two layers were found to be highly ordered, crystalline phases. Bilayer crystallization accompanied by some molecular reorientation is believed to also occur in the N_2−graphite system at low temperatures.[29] At much higher temperatures, the first two layers may not be as highly ordered. The q_{st} for other carbon-adsorbate systems[30−32] is generally higher than that for the MWNT−adsorbate system.[31,33] For example, adsorption of various alkanes on different carbon blacks displayed initial heats of adsorption approximately 3 times larger than their isosteric heat of condensation.[13] In our case, the initial heat of adsorption is at most 1.3 times the butane heat of condensation, as can be seen in Figure 5.

Adsorption of gases on graphite might be considered as a limiting case of adsorption on MWNTs in the limit of zero curvature of the surface. According to the Kelvin equation (eq 2), the vapor pressure over a convex surface should be higher than it is over a flat surface, which may serve as a reasonable explanation for the lower isosteric heats of adsorption. It has been reported that the monolayer Kr condensation pressures over MWNT surfaces are higher than those observed over graphite, which is consistent with what is predicted by the Kelvin equation.[30,33] The higher condensation pressure probably leads to an incomplete wetting of the surface by limiting the numbers of Kr monomolecular layers adsorbed before its bulk condensation.[33] The presence of surface impurities in the form of amorphous carbon has been detected on our MWNT samples from TEM photos; these impurities will increase the heterogeneity of our samples and thus decrease the heat of adsorption.

On the other hand, a highly bent graphite sheet, such as the wall in a carbon nanotube, has strained double bonds, resulting in a sp^2/sp^3 orbit-hybridization. Recent EELS experiments show that the curvature must be extensive to lead to a measurable hybridization;[34−39] thus the effect has only been observed in SWNTs, but not in MWNTs. SWNTs display a high surface potential not only inside the pore relative to a flat graphite surface,[40] but also on the outer wall of the tube. Orbital or potential overlaps between surfaces that are sufficiently close to each other, such as the graphite sheets in graphite,[9] can result in slit condensation. Large pore volumes and strained surface bonds give two possible explanations as to why the binding energy for a gas adsorbed on both closed and open-ended SWNTs[41−47] generally is much higher than it is on planar graphite[48] and other types of carbon.[49−52]

Methane adsorption on close-ended SWNTs was found to display a binding energy, ϵ_B, 76% larger than that for planar

TABLE 2: Log-Normal Distribution Model Function Parameters and Modified BET Parameters for Three Samples with Well-Defined Morphology[5]

sample	μ	σ	d [nm]	n_m [mg/g]	K	C
A	3.21	0.730	24.4	13.54	0.75	161
B	3.57	0.903	48.5	6.90	0.73	132
C	3.96	0.944	52.2	4.56	0.69	212

graphite.[53,54] The adsorption capacity was also found to be higher, possibly due to a larger number of carbon atoms neighboring each adsorbed molecule in the interstitial channels, as compared to adsorption on a flat graphite surface. In another investigation ϵ_B was found to be ~60% larger for He on SWNTs.[55] The same type of result has also been found for H_2 and Ne in SWNTs, where the binding energy was calculated to be ~150% larger than that for graphite.[40,56−58] Either He and methane are too large to adsorb into the interstitial channels and only adsorb in the groove sites, or the larger molecules do access the interstitial channels and the number of favorable sites is smaller for larger molecules. (One molecular dynamics study suggests that SWNTs can expand to hold xylene, a relatively large molecule.[59])

Collected literature data show that the butane[5] and ethane[31] isosteric heat of adsorptions are consistently lower for adsorption on MWNTs than on graphite,[31,32,60−63] confirming that the surface strain is not sufficient to create orbital hybridization and that the pore density is too low to have any impact on q_{st}. The isosteric heat of adsorption for the Kr-MWNT system is also lower than that for the Kr−graphite system.[30, 33]

Relating MWNT Morphology and Adsorption Capacity. Since the adsorption of butane on MWNTs is well-described by the BET equation, we should be able to use butane adsorption data to estimate the nanotube morphology. We have previously shown that our MWNT inner and outer MWNT diameters could be fitted using a two-parameter log-normal probability distribution model:[5]

$$f(\ln(d),\mu,\sigma) = \frac{1}{2\pi\sigma} e^{-((\ln(d)-\mu)^2/2\sigma^2)} \quad (4)$$

The parameters μ and σ correspond to the distribution logarithmic mean and standard deviation. The MWNTs of this study and our prior work should all have the same relationships between the mean diameter, the standard deviation of the diameter, and the value for monolayer coverage, n_m, since our CVD process makes MWNTs with reproducible morphologies. Thus, we should be able to calculate the parameters μ and σ for samples 1−3 by using data collected from MWNT samples with well-known morphology. Three such samples, samples A−C, already exist and can been used in an attempt to find μ and σ as a functions of n_m. The samples have mean diameters of 24.4, 48.5, and 52.2 nm, respectively, and are presented in detail in Table 2 below.

If we plot μ and σ for samples A and B vs n_m (see Figure 6), the empirical linear relations between the log-normal probability distribution parameters and n_m at 298.15 K are linear and can be described as:

$$\mu = -89.2 n_m + 4.4 \quad (5a)$$

$$\sigma = -40.9 n_m + 1.1 \quad (5b)$$

R^2 values are 0.97 for both μ and σ. From these simple relations, σ and μ can be estimated from n_m at 298.15 K for samples 1−3. Table 3 displays the external diameter mean and standard deviation for samples 1−3 as calculated from eq 5a,b.

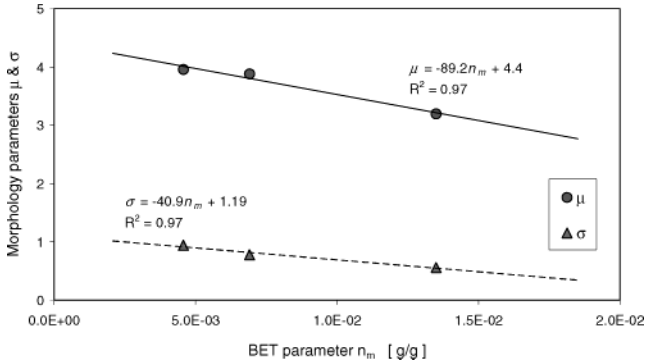

Figure 6. The log-normal parameters σ and μ, for three known samples, fitted as linear functions of their corresponding BET parameter n_m.

TABLE 3: Morphology Parameters Calculated from Empirical Linear Relations with n_m for Samples 1, 2, and 3 at 298 K

sample	μ	σ	diameter [nm]
1	3.66	0.886	39.1
2	3.73	0.907	41.7
3	3.81	0.933	45.2

TABLE 4: Comparison between Experimental and Predicted n_m (Eq 5a,b)[a]

sample	exptl n_m [mg/g]	predicted n_m [mg/g]	exptl n_m [mg/m^2]	d_{butane} [Å]
1	6.7	4.9	0.40	2.43
2	6.0	4.3	0.39	2.44
3	5.2	4.0	0.38	2.49

[a] The butane packing diameter is estimated by assuming a square lattice packing of butane on the external surface.

We have previously established that the inner diameter distribution is independent of outside diameter and the mean changes little from sample or within one sample. As a correlative calculation, n_m was calculated from the distribution model, using a simple geometrically based equation:[5]

$$n_{m,pred} = k \frac{\sum_{n=1}^{n} (D_O + 2R_g)}{\sum_{n=1}^{n} (D_O^2 - D_I^2)} = k \frac{\int_0^\infty f(\ln(D_O),\mu,\sigma)\,(D_O + 2R_g)\,dD_O}{\int_0^\infty f(\ln(D_O),\mu,\sigma)\,(D_O^2 - D_I^2)\,dD_O} \text{ g/g} \quad (6)$$

The constant k is

$$k = \frac{M_{C4}}{N_A \cdot \rho_C \cdot R_g^2} \text{ g·m/g}$$

D_O and D_I are the MWNT outer and inner diameter, respectively, M_{C4} and R_g are the butane molar mass and radius of gyration, N_A is Avogadro's constant, and ρ_c is the density of graphite. The function, f, is the log-normal distribution equation (eq 4).

The calculated n_m values (Table 4) were plotted vs the measured n_m for all six samples (Figure 7). Sample 6 has a much smaller radius than the other materials, and may have a different percentage of surface defects.

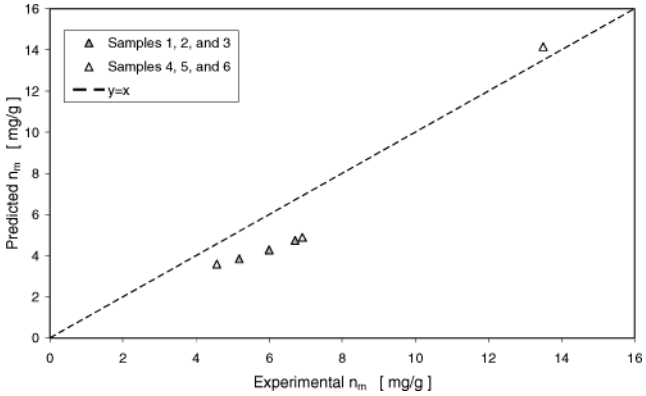

Figure 7. The predicted n_m values (eq 5a,b) for the five samples with larger diameters are about 30% lower than the experimental value for n_m.

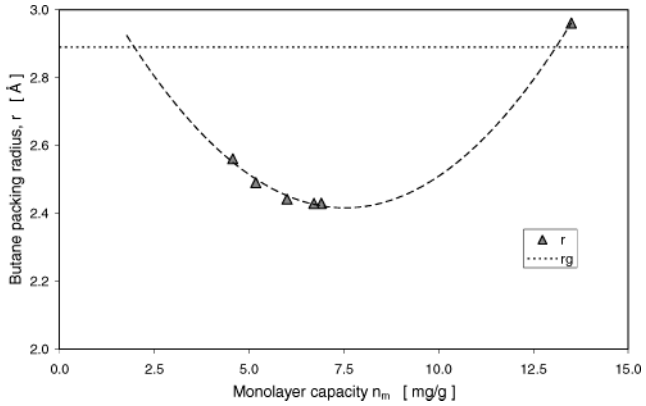

Figure 8. The estimated butane packing radius, calculated by iterating n_m. The dotted line across the graph indicates the standard butane radius of gyration, which is 2.89 Å.

Adsorbate Order and Orientation. We calculated the butane packing radius by iterating eq 6 to fit the measured monolayer capacity, n_m. The procedure was carried out for all six samples and the result is plotted in Figure 8. The dotted horizontal line in Figure 8 represents the butane radius of gyration, 2.89 Å.

The packing radius ranges between ~2.4 and 2.6 Å for the larger tubes. For the smallest MWNTs, the butane radius is closer to 3 Å. If we assume a square packing, the surface areas are ~23−27 Å^2/butane molecule for the larger tubes. The sample with the smallest mean diameter is occupied by butane molecules each taking up an area of 36 Å^2. The latter number is very close to values already reported in the literature for butane on carbon black[13] and graphite:[28,63] ~30−40 Å^2.

From n_m it is possible to determine the area occupied by each butane molecule on the MWNT external surface. Assuming a square butane packing lattice, the area per molecule is calculated to lie between 26 and 32 Å^2. For five of the six samples analyzed, the estimated areas were found to be smaller than values previously reported in the literature. These five samples had larger average diameters. If the calculated areas are plotted vs corresponding n_m, a minimum seems to occur for the two samples with average diameters of 48.5 and 48.7 nm, respectively.

Several studies suggest that the preferred equilibrium orientation for a hydrocarbon physisorbed on a graphitic surface is parallel to the wall.[8,63,64] If we assume that butane is 7.01 Å long and 3.059 Å wide, the packing would have to be very tight to enable a horizontal butane orientation relative to the MWNT surface. It is more likely that the molecules are slightly tilted from the surface, but more detailed studies are necessary to clarify this issue. The volume for a solid butane phase is about 120−125 Å^3 (DIPPR), which is a 5 Å/side cube, or a 6-Å-diameter sphere, so the estimated areas are not unreasonable. Computer simulations suggest that the principal mechanism for vacancy creation for butane in the already adsorbed monolayer is tilting of the molecule axis away from the basal plane of graphite.[65,66] Also, when butane is adsorbed on top of the tightly packed butane monolayer, the molecules tilt out-of-plane by 22°, indicating the existence of a crystalline bilayer.[27]

Structured Carbons for Gas Separations. The selectivity of slit pore graphites for binary gas separations is a function of the orientation of molecules in the spacing between the pore walls.[67−69] Microporous materials can exhibit quantum sieving, where heavy isotopes are preferentially adsorbed over light isotopes (H_2-T_2, ^{3}He-^{4}He, CH_4-CD_4, and H_2-HD[70,71]). Predictions of isotherms and selectivities can be evaluated by using the enthalpy of vaporization of the components and their heats of adsorption.[72] Some binary separations have been proposed for SWNTs: $CClF_2CF_3$ from CHF_2CF_3[73] and H_2 from CO.[74] The geometrical pore properties of the SWNT sample, such as size or shape, affect separations as do the energetics of the adsorbate surface.[74]

The relatively pure MWNTs used in this study adsorb butane via a physisorption mechanism, condensing a number of adsorbate monolayers at relative pressures near 0.9. Separations of binary pairs of gases would depend on their differences in surface condensation for specific temperatures and partial pressures in the adsorption system. Since no hysteresis is observed, thermal or pressure swing adsorption cycles could be effective for recovery of adsorbed and condensed gases.

Conclusions

Butane adsorption on MWNTs generated isotherms of type II, which is defined as physisorption on solid (nonporous) surfaces. Capillary condensation may not be detectable, since it occurs over a wide relative pressure range ($p/p^o = 0.3-0.93$ for $d = 2-12$ nm) and no more than 0.5 wt % of the total mass uptake is condensed in the pores of the samples. The wide pressure range and the small relative pore condensation may also explain why hysteresis was not observed in any of the sample's adsorption/desorption cycles. Another possible explanation is that for the majority of the MWNTs, only one end is accessible to the atmosphere. A simple correlation between monolayer coverage and MWNT morphology allows the prediction of a sample's morphology from the measured sample monolayer capacity, n_m. The developed method eliminates time-consuming and challenging MWNT morphology measurements and greatly simplifies the MWNT analysis process.

The isosteric heat of adsorption, q_{st}, was calculated from each isotherm-set by applying the Clausius−Clapeyron equation. The magnitude of q_{st} confirms that the adsorption mechanism is physisorption. The heat of adsorption was highest at low levels of surface coverage and decreased steadily until a minima was reached at $\theta = 1$. This result indicates that our MWNT samples are heterogeneous adsorbents. TEM pictures confirm the presence of surface impurities in the form of amorphous carbon. For $\theta > 2.5$, the isosteric heat of adsorption is approaching the butane heat of condensation.

Adsorption on MWNTs is less energetically favorable compared to adsorption on flat graphite. The initial heats of adsorption were found to lie between 22 and 26 kJ/mol, which is around $^2/_3$ of reported q_{st} values for butane adsorption on graphite. MWNT surface impurities, such as amorphous carbon, probably lower the surface potential. It seems likely that the

butane packing differs between each adsorbed layer on the MWNT wall, with the butane molecules tilting away from the surface perpendicular. On the other hand, SWNT surfaces seem to be more attractive than graphite, but there is lack of agreement between groups as to why. Our results demonstrate that the key to understanding adsorption on nanotubes is to carefully research the adsorbent to determine surface area, pore volume, and the presence of defects.

Acknowledgment. The authors acknowledge the support of the National Science Foundation (98-09686) for this work and thank Rodney Andrews and David Jacques of the Center for Applied Energy Research for the MWNT samples and the use of the Hiden equipment.

References and Notes

(1) Hilding, J.; et al. Dispersion of carbon nanotubes in liquids. In *J. Dispersion Sci. Technol.* **2003**, *24* (1), 1−41.

(2) Journet, C.; et al. Large-scale production of single-walled carbon nanotubes by the electric-arc technique. In *Nature* (*London*) **1997**, *388*, 756−758.

(3) Kiang, C.-H.; et al. Carbon nanotubes with single-layer walls. In *Carbon* **1995**, *33*, 903−914.

(4) Thess, A.; et al. Crystalline ropes of metallic carbon nanotubes. In *Science* (*Washington, D.C.*) **1996**, *273*, 483−487.

(5) Hilding, J.; et al. Sorption of butane on carbon multiwall nanotubes at room temperature. In *Langmuir* **2001**, *17*, 7540−7544.

(6) Ajayan, P. M. Nanotubes from Carbon. In *Chem. Rev.* (*Washington, D.C.*) **1999**, *99*, 1787−1799.

(7) Jacques, D.; et al. Synthesis of multiwalled carbon nanotubes. In *Mater. Res. Soc. Symp. Proc.* **2000**, *593*, 15−20.

(8) Andrews, R.; et al. Continuous production of aligned carbon nanotubes: a step closer to commercial realization. In *Chem. Phys. Lett.* **1999**, *303* (5−6), 467−474.

(9) Gregg, S. J.; Sing, K. S. W. *Adsorption, Surface Area and Porosity*, 2nd ed.; Academic Press Inc.: New York, 1982.

(10) Aveyard, R. H., D. A. *An introduction to the principles of surface chemistry*; UK: Syndics of the Cambridge University Press: London, 1973.

(11) Daubert, T. E., Danner, R. P., Eds. *Physical and Thermodynamic Properties of Pure Chemicals*: *Data Compilation*; Hemisphere: New York, 1989.

(12) Brunauer, S.; Skalny, J.; Bodor, E. E. Adsorption on nonporous solids. In *J. Colloid Interface Sci.* **1969**, *30*, 546−552.

(13) Beebe, R. A.; et al. Heats of adsorption on carbon black. II. In *J. Am. Chem. Soc.* **1947**, *69*, 2294−2299.

(14) Inoue, S.; et al. Capillary Condensation of N2 on Multiwall Carbon Nanotubes. In *J. Phys. Chem. B* **1998**, *102*, 4689−4692.

(15) Mackie, E. B.; et al. Adsorption Studies of Methane Films on Catalytic Carbon Nanotubes and on Carbon Filaments. In *Langmuir* **1997**, *13*, 7197−7201.

(16) Meichel, T.; et al. Adsorption of ethylene on graphite near saturation: wetting transition/capillary condensation. In *Langmuir* **1990**, *6*, 1579−1584.

(17) Piper, J.; Morrison, J. A. Heats of adsorption of methane multilayers on graphite. In *Phys. Rev. B*: *Condens. Matter Mater. Phys*. **1984**, *30*, 3486−3489.

(18) Mann, D. J.; Halls, M. D. Ab initio simulations of oxygen atom insertion and substitutional doping of carbon nanotubes. In *J. Chem. Phys*. **2002**, *116*, 9014−9020.

(19) Zhou, L. G.; Shi, S. Q. Adsorption of foreign atoms on Stone-Wales defects in carbon nanotube. In *Carbon* **2003**, *41*, 613−615.

(20) Lee, H.; et al. Hydrogen desorption properties of multiwall carbon nanotubes with closed and open structures. In *Appl. Phys. Lett.* **2002**, *80*, 577−579.

(21) Zhang, H.-B.; et al. Raman spectra of MWCNTs and MWCNT-based H2-adsorbing system. In *Carbon* **2002**, *40*, 2429−2436.

(22) Kim, J.; No, K.; Lee, C. J. Growth and field emission of carbon nanotubes on electroplated Ni catalyst coated on glass substrates. In *J. Appl. Phys*. **2001**, *90*, 2591−2594.

(23) Sibrell, P. L.; Miller, J. D. Significance of graphitic structural features in gold adsorption by carbon. In *Mineral. Metallurgical Proc*. **1992**, *9*, 189−95.

(24) Sattler, K. STM of anomalous carbon structures. In *Int. J. Modern Phys. B* **1992**, *6* (23−24), 3603−3612.

(25) Au, C. T.; Hirsch, W.; Hirschwald, W. Adsorption of carbon monoxide and carbon dioxide on annealed and defect zinc oxide (000.hivin.1) surfaces studied by photoelectron spectroscopy (XPS and UPS). In *Surf. Sci*. **1988**, *197*, 391−401.

(26) Jakob, P.; Gsell, M.; Menzel, D. Interactions of adsorbates with locally strained substrate lattices. In *J. Chem. Phys*. **2001**, *114*, 10075−10085.

(27) Herwig, K. W.; Newton, J. C.; Taub, H. Structure and growth of butane films adsorbed on graphite. In *Phys. Rev. B*: *Condens. Matter* **1994**, *50*, 15287−15297.

(28) Alkhafaji, M. T.; Migone, A. D. Heat-capacity study of butane on graphite. In *Phys. Rev. B*: *Condens. Matter* **1996**, *53*, 11152−11158.

(29) Wang, S. K.; et al. Multilayer structure of nitrogen adsorbed on graphite. In *Phys. Rev. B*: *Condens. Matter Mater. Phys.* **1989**, *39*, 10331−10341.

(30) Putnam, F. A.; Fort, T., Jr. Physical adsorption of patchwise heterogeneous surfaces. I. Heterogeneity, two-dimensional phase transitions, and spreading pressure of the krypton-graphitized carbon black system near 100 deg K. In *J. Phys. Chem*. **1975**, *79*, 459−467.

(31) Masenelli-Varlot, K.; McRae, E.; Dupont-Pavlovsky, N. Comparative adsorption of simple molecules on carbon nanotubes Dependence of the adsorption properties on the nanotube morphology. In *Appl. Surf. Sci*. **2002**, *196* (1−4), 209−215.

(32) Inaba, A.; Morrison, J. A. Ethylene on graphite: heats of adsorption and phase diagram. In *Physi. Rev. B*: *Condens. Matter Mater. Phys*. **1986**, *34*, 3238−3242.

(33) Bougrine, A.; et al. Comparison of the adsorption properties of krypton on multi-walled carbon nanotubes and on graphite. In *Mater. Res. Soc. Symp. Proc.* **2001**, *633*, A14.7.1−A14.7.6.

(34) Stephan, O.; et al. Curvature-induced bonding changes in carbon nanotubes investigated by electron energy-loss spectrometry. In *Phys. Rev. B*: *Condens. Matter* **1996**, *53*, 13824−13829.

(35) Reed, B. W.; et al. Transmission electron energy-loss spectroscopy study of carbon nanotubes upon high-temperature treatment. In *Appl. Phys. Lett.* **2001**, *78*, 3358−3360.

(36) Botton, G. A.; et al. Microstructural and electron spectroscopic characterization of carbon nanostructures and nanotubes produced using multimetal catalysts. In *J. Phys. Chem. Solids* **1997**, *58*, 1091−1102.

(37) Knupfer, M.; et al. Electron energy-loss spectroscopy studies of single wall carbon nanotubes. In *Carbon* **1999**, *37*, 733−738.

(38) Stephan, O.; et al. Electron energy-loss spectroscopy on individual nanotubes. In *J. Electron Spectrosc. Relat. Phenom.* **2001**, *98*, 209−217.

(39) Yase, K.; et al. Angular-resolved EELS of a carbon nanotube. In *Thin Solid Films* **1996**, *273* (1−2), 222−224.

(40) Stan, G.; et al. Atoms in nanotubes: small dimensions and variable dimensionality. In *Am. J. Phys*. **1999**, *67*, 1170−1176.

(41) Talapatra, S.; Migone, A. D. Adsorption of methane on bundles of closed-ended single-wall carbon nanotubes. In *Phys. Rev. B*: *Condens. Matter Mater. Phys*. **2002**, *65*, 045416/1−045416/6.

(42) Talapatra, S.; et al. Gases Do Not Adsorb on the Interstitial Channels of Closed-Ended Single-Walled Carbon Nanotube Bundles. In *Phys. Rev. Lett.* **2000**, *85*, 138−141.

(43) Zambano, A. J.; Talapatra, S.; Migone, A. D. Binding energy and monolayer capacity of Xe on single-wall carbon nanotube bundles. In *Phys. Rev. B*: *Condens. Matter Mater. Phys*. **2001**, *64*, 075415/1−075415/6.

(44) Pradhan, B. K.; et al. Experimental probes of the molecular hydrogen−carbon nanotube interaction. In *Phys. B: Condens. Matter* (*Amsterdam, Netherlands*) **2002**, *323* (1−4), 115−121.

(45) Wei, B.-Y.; et al. Gases adsorption on single-walled carbon nanotubes measured by piezoelectric quartz crystal microbalance. In *Mater. Chem. Phys*. **2003**, *81*, 126−133.

(46) Yoo, D.-H.; et al. Study of nitrogen adsorbed on single-walled carbon nanotube bundles. In *J. Phys. Chem. B* **2002**, *106*, 3371−3374.

(47) Yoo, D.-H.; et al. Study of Nitrogen Adsorbed on Open-Ended Nanotube Bundles. In *J. Phys. Chem. B* **2003**, *107*, 1540−1542.

(48) Vidali, G.; et al. Potentials of physical adsorption. In *Surf. Sci. Rep*. **1991**, *12*, 133−181.

(49) Pace, E. L.; Siebert, A. R. Heat of adsorption of parahydrogen and orthodeuterium on Graphon. In *J. Phys. Chem*. **1959**, *63*, 1398−1400.

(50) Beebe, R. A.; et al. Heats of adsorption on carbon black. I. In *J. Am. Chem. Soc*. **1947**, *69*, 95−101.

(51) Piper, J.; et al. Heats and entropies of adsorption of nitrogen on Grafoil at 79.3 K. In *J. Chem. Soc., Faraday Trans. 1* **1983**, *79*, 2863−2874.

(52) Gale, R. L.; Beebe, R. A. Determination of heats of adsorption on carbon black and bone mineral by chromatography using the eluted pulse technique. In *J. Phys. Chem.* **1964**, *68*, 555−567.

(53) Weber, S. E.; et al. Determination of the binding energy of methane on single-walled carbon nanotube bundles. In *Phys. Rev. B*: *Condens. Matter Mater. Phys.* **2000**, *61*, 13150−13154.

(54) Weber, S.; et al. Direct measurement of binding energy via adsorption of methane on SWNT. In *Science and Application of Nanotubes*; Proceedings of Nanotube '99, an International Conference, East Lansing, MI, July 24−27, 1999; published in 2000; pp 215−221.

(55) Teizer, W.; et al. 4He Desorption from Single Wall Carbon Nanotube Bundles: A One-Dimensional Adsorbate. In *Phys. Rev. Lett.* **1999**, *82* (26, Pt. 1), 5305−5308.

(56) Stan, G.; Cole, M. W. Low coverage adsorption in cylindrical pores. In *Surf. Sci.* **1998**, *395* (2/3), 280−291.

(57) Stan, G.; et al. Interstitial He and Ne in nanotube bundles. In *J. Low-Temp. Phys.* **1998**, *113* (3/4), 447−452.

(58) Stan, G.; Cole, M. W. Hydrogen adsorption in nanotubes. In *J. Low-Temp. Phys.* **1998**, *110* (1/2), 539−544.

(59) Takaba, H.; et al. Molecular design of carbon nanotubes for the separation of molecules. In *Microporous Mater.* **1995**, *3* (4−5), 449−455.

(60) Chirnside, G. C.; Pope, C. G. Limiting isosteric heats of adsorption of *n*-butane, *n*-pentane, and *n*-hexane on graphitized carbon black. In *J. Phys. Chem.* **1964**, *68*, 2377−2379.

(61) Ross, S.; Saelens, J. K.; Olivier, J. Physical adsorption. XVIII. Limiting isosteric heats of adsorption of gases on graphitized carbon by the chromatographic method. In *J. Phys. Chem.* **1962**, *66*, 696−700.

(62) Kiselev, A. V. Surface chemistry, adsorption energy, and adsorption equilibriums. In *Q. Rev.* (*London*) **1961**, *15*, 99−124.

(63) Hoory, S. E.; Prausnitz, J. M. Adsorption of hydrocarbons on graphitized carbon. In *Trans. Faraday Soc.* **1967**, *63*, 455−460.

(64) Battezzati, L.; Pisani, C.; Ricca, F. Equilibrium conformation and surface motion of hydrocarbon molecules physisorbed on graphite. In *J. Chem. Soc., Faraday Trans. 2* **1975**, *71*, 1629−1639.

(65) Hansen, F. Y.; Taub, H. Melting mechanism in monolayers of flexible rod-shaped molecules. In *Phys. Rev. Lett.* **1992**, *69*, 652−655.

(66) Hansen, F. Y.; Newton, J. C.; Taub, H. Molecular-dynamics studies of the melting of butane and hexane monolayers adsorbed on the basal-plane surface of graphite. In *J. Chem. Phys.* **1993**, *104*, 4128−4141.

(67) Nicholson, D. Using computer simulation to study the properties of molecules in micropores. In *J. Chem. Soc., Faraday Trans.* **1996**, *92*, 1−9.

(68) Cracknell, R. F.; Nicholson, D. Grand canonical Monte Carlo study of Lennard-Jones mixtures in slit pores. In *J. Chem. Soc., Faraday Trans.* **1994**, *90*, 1487−1493.

(69) Cracknell, R. F.; Nicholson, D.; Gubbins, K. E. Molecular dynamics study of the self-diffusion of supercritical methane in silt-shaped graphitic micropores. In *J. Chem. Soc., Faraday Trans.* **1995**, *91*, 1377−1383.

(70) Challa, S. R.; Sholl, D. S.; Johnson, J. K. Light isotope separation in carbon nanotubes through quantum molecular sieving. In *Phys. Rev. B: Condens. Matter Mater. Phys.* **2001**, *63*, 245419/1−245419/9.

(71) Wang, Q.; et al. Quantum Sieving in Carbon Nanotubes and Zeolites. In *Phys. Rev. Lett.* **1999**, *82*, 956−959.

(72) Aranovich, G. L.; Donohue, M. D. Adsorption of Chain Molecules. In *J. Colloid Interface Sci.* **1999**, *213*, 457−464.

(73) Corbin, D. R.; Reutter, D. W. Adsorptive purification of pentafluoroethane from its mixtures with chloropentafluoroethane using carbon nanotubes. In *U.S. 1997*; E. I. Du Pont De Nemours and Company, USA; 4 pp.

(74) Nicholson, D.; Gubbins, K. E. Separation of carbon dioxide-methane mixtures by adsorption: effects of geometry and energetics on selectivity. In *J. Chem. Phys.* **1996**, *107*, 8126−8134.